

We are IntechOpen, the world's leading publisher of Open Access books Built by scientists, for scientists

6,900

Open access books available

186,000

International authors and editors

200M

Downloads

Our authors are among the

154

Countries delivered to

TOP 1%

most cited scientists

12.2%

Contributors from top 500 universities



WEB OF SCIENCE™

Selection of our books indexed in the Book Citation Index
in Web of Science™ Core Collection (BKCI)

Interested in publishing with us?
Contact book.department@intechopen.com

Numbers displayed above are based on latest data collected.
For more information visit www.intechopen.com



Phage Capsids as Gated, Long-Persistence, Uniform Drug Delivery Vehicles

Philip Serwer, Elena T. Wright and Cara B. Gonzales

Abstract

Over the last 25 years, cancer therapies have improved survivorship. Yet, metastatic cancers remain deadly. Therapies are limited by inadequate targeting. Our goal is to develop a new drug delivery vehicle (DDV)-based strategy that improves targeting of drug delivery to solid tumors. We begin with a capsid nanoparticle derived from bacteriophage (phage) T3, a phage that naturally has high persistence in murine blood. This capsid has gating capacity. For rapidly detecting loading in this capsid, here, we describe procedures of native agarose gel electrophoresis, coupled with fluorescence-based detection of loaded molecules. We observe the loading of two fluorescent compounds: the dye, GelStar, and the anticancer drug, bleomycin. The optimal emission filters were found to be orange and green, respectively. The results constitute a first milestone in developing a drug-loaded DDV that does not leak when in blood, but unloads its cargo when in a tumor.

Keywords: agarose gel electrophoresis, bacteriophage T3, bleomycin, buoyant density centrifugation, capsid impermeability, GelStar

1. Introduction

Current therapies for cancerous tumors suffer from both toxic secondary effects and the development by the tumor of drug resistance. These effects usually block therapy for metastatic cancers, the cause of 90% of cancer deaths [1–5]. For solving these problems, our first thesis is that the best strategy is to increase tumor specificity of anticancer drug delivery in several, *independent* stages. If, for example, three stages are used and each stage is 80% efficient (20% nonefficient) in increasing specificity, then overall efficiency is 99% [$100 \times (1.0 - 0.2^3)$]. In this case, (1) drug dosages to tumors can be raised 100× without changing toxicity and, therefore, (2) tumor cell evolution of drug resistance is minimized.

The primary alternative is to continue testing chemotherapies [6–8], immunotherapies [9–11] and radiotherapies [12–14] that have tumor-specificity determined at one independent stage. This one stage is often cellular DNA replication, which is more rapid and, therefore, more drug- and radiation-sensitive, in cancerous cells than it is in healthy cells. One-stage strategies are >100 years old for immunotherapy and radiotherapy. Chemotherapeutic agents typically used are over 50 years old [8]. Even major effort has not produced systematic therapies for metastatic cancer.

Apparently, new, possibly more biology-based, strategy is needed to counter risk that the above one-stage-based strategies, in general, are not realistic for reaching objectives (reviewed in [1, 15–17]).

In theory, one implementation of multi-stage strategy starts with drug delivery in a drug delivery vehicle (DDV) that is gated. The gate is opened to load drug, closed in circulation to deliver drug and opened again in tumors to administer drug. Stages of DDV-derived toxicity reduction are the following tumor-specific events: (1) DDV delivery, (2) DDV opening and, (3) drug activation, for masked drugs. We address stages (1) and (2) here.

In this implementation, tumor-specific delivery is achieved via the EPR effect. The EPR effect is the spontaneous accumulation of nanoparticles in tumors, observed for an uncharacterized phage in 1940 [18] (reviewed in [19]). The causes of the EPR effect are (1) porosity of tumor blood vessels and relative tightness of healthy blood vessels, so that nanoparticles enter tumors, but usually not healthy tissue and (2) poor tumor lymphatic drainage, so that nanoparticles remain [20–25]. The EPR effect is the basis for the use of several FDA-approved, drug-loaded, liposomal DDVs [23, 24, 26].

However, circulating, drug-loaded, liposomal DDVs undergo drug leakage that causes significant toxicity [22, 23, 25, 27]. Also, liposomes are removed from circulation by the macrophage-phagocyte innate immune system. That is to say, liposomes are not very persistent. Chemical solutions to the leakage problem do not exist to our knowledge. Chemical solutions to the persistence problem (e.g., polyethylene glycol derivatization [28, 29]) introduce quality control problems and are not adaptable to future improvements, for example, achieving of tumor-specific unloading. The second thesis is that the optimal solution is linked to finding an appropriate, biologically produced, microbial DDV. Unlike some biology-based anticancer strategies [1, 15, 16, 19], use of a DDV is implementable with nononcolytic viruses and, therefore, avoids the dangers [19] of using oncolytic viruses.

In practice, we have discovered a phage T3 capsid that appears to have DDV-favorable characteristics needed for implementation of our strategy. First, phage T3 (and presumably its capsid) has recently been found to have exceptionally high persistence in mouse blood (3–4 h), unlike the T3 relative, T7 [30]. Second, one empty, but otherwise phage-like T3 capsid, is impermeable (for over 20 years) to the compound, Nycodenz (821 Da molecular weight) (reviewed in [31]). But, when the temperature is raised to 45°C, Nycodenz enters this capsid [32], presumably through a gate that opened. The concept is that, if we adapt this capsid to use as gated DDV, some of the needed engineering has already been done by natural selection.

Phages T3 and T7 are illustrated at the left in **Figure 1**. The gated capsid is illustrated at the right in **Figure 1**. This capsid is generated during DNA packaging that had been initiated by a DNA-free procapsid called capsid I (not shown). During packaging, capsid I expands and becomes the more angular and stable capsid (capsid II) illustrated in **Figure 1**. In nature, the capsid-gate is a ring of 12 gp8 molecules (**Figure 1**) that acts as entry portal for DNA during DNA packaging [31–33]. Most T3 and T7 capsid II particles are purified after having detached from DNA during infected cell lysis. The amount is 5–10 mg capsid II per liter of culture. The last purification step is buoyant density centrifugation in a Nycodenz or Metrizamide density gradient. Nycodenz low density (NLD) capsid II has the gp8 “gate” and is impermeable to Nycodenz and Metrizamide. The low density (1.08 g/ml) is caused by high internal hydration, which is caused by Nycodenz impermeability.

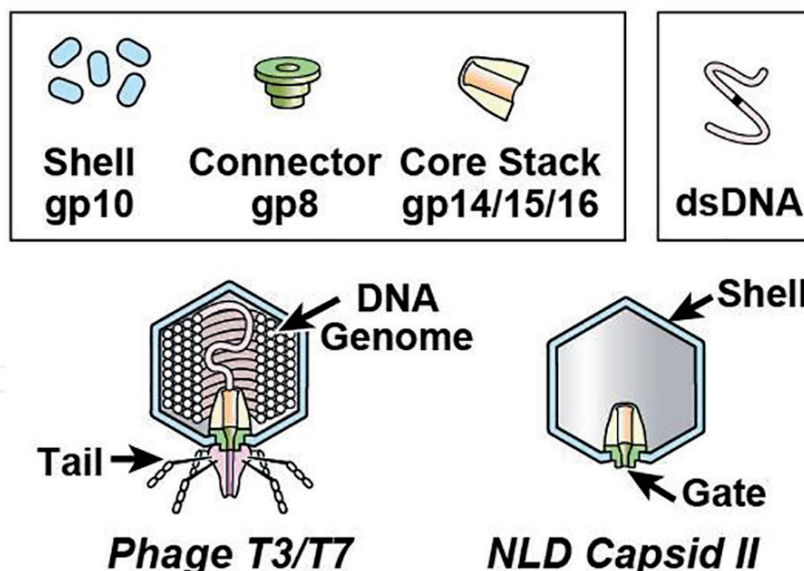


Figure 1. Phages T3 and T7 (left); and T3 and T7 NLD capsid II (right). The graphic legend at the top indicates the various capsid components. A protein is labeled by gp, followed by the number of the encoding gene. Analogous T3 and T7 genes have the same numbers. If NLD capsid II is used as DDV, the perimeter of the DDV is defined by the gp10 shell; the gate is the gp8 portal. All structures are the same for phage T3 as they are for phage T7 (reviewed in [31, 32]).

Nycodenz high density (NHD) capsid II is Nycodenz-permeable (1.28 g/ml) and is completely separated from NLD capsid II during buoyant density centrifugation in a Nycodenz or Metrizamide density gradient [31, 33–35]. We use NHD capsid II as a control during loading experiments.

In the case of T3 NLD capsid II, gated entry of Nycodenz has been observed via raising of temperature. The likely entry channel was the axial hole of the gp8 ring. This conclusion was drawn, in the case of T7 NLD capsid II, from (1) entry kinetics of the fluorescent dye, bis-ANS [1,1'-bi(4-anilino)naphthalene-5,5'-di-sulfonic acid; 673 Da], and (2) covalent cross-linking of bis-ANS to channel proteins [33]. Asymmetric reconstruction-cryo-EM [36] revealed that obstruction of the T7 gp8 channel (and presumably the T3 channel) varies.

In support of working to implement the above gating-based strategy, the following quote from 2005 presents an expert opinion of what is needed for the next generation of anticancer DDVs [27]. “An ideal liposomal anticancer drug would exhibit little or no drug release while in the plasma compartment, thus ensuring limited exposure of the drug to healthy tissue. This feature would also maximize drug delivery to disease sites, as mediated by the movement of the drug-loaded liposomes from the plasma compartment to the extravascular space at disease sites, such as a region of tumor growth. Following localization, however, the drug-loaded liposome must transform itself from a stable carrier to an unstable carrier. This would ensure that the drug, which has localized in the diseased site, is bioavailable.” To our knowledge, no details for such “controlled release” via a liposomal DDV have been published. The system described here is designed to accomplish what is described in the above quote. However, implementation uses gating of a DDV, not programmed instability of a DDV.

To proceed further, we need a procedure for rapidly determining whether a drug is loaded in a capsid. In the current study, we have developed native agarose gel electrophoresis (AGE) for this purpose. The detection is performed via capsid band fluorescence produced by the compound loaded.

2. Results

2.1 Detection of test compounds: GelStar

We tested the loading of two fluorescent compounds. The first was GelStar, a fluorescent nucleic acid stain typically used after AGE. In contrast, we incubated GelStar with our capsid and then performed AGE without further use of GelStar. The second compound was bleomycin, an anticancer drug [37, 38] that is also fluorescent [38]. Neither the manufacturer nor the vendor provided either the structure of GelStar or the concentration of commercial GelStar solutions. GelStar is sold in solution only.

The dominant fluorescence emission of nucleic acid-bound GelStar is in the green range. Apparently not previously documented is that the dominant fluorescence emission of free GelStar is in the orange range, at least when the GelStar is in an agarose gel. Ultraviolet light stimulated GelStar fluorescence emission vs. GelStar dilution is shown in **Figure 2**. Free GelStar, at several dilutions, had been pipetted in 5 μl amounts onto an agarose gel before ultraviolet light illumination and photography through an orange filter (spots labeled G in **Figure 2**). The effective volume in μl (dilution, multiplied by 5) of the stock GelStar solution is also indicated. In **Figure 2**, the color of GelStar spots is orange for all dilutions, as it also is found to be (not shown) with yellow and green emission filters. The orange color is real and is not produced by the emission filter because green Alexa 488 dye fluorescence retains its green color (spots labeled A in **Figure 2**). The number next to the Alexa 488 spots is the total amount (μg) of Alexa 488, also applied in 5 μl amounts.

DNA-bound GelStar had the expected green emission at all dilutions, when viewed through the same orange emission filter used for **Figure 2** (right side of the right panel of **Figure 3**). Green emission was also dominant when yellow and green emission filters were used for DNA-bound GelStar (not shown).

2.2 Detection of test compounds: bleomycin

Without fluorescent compound, the background of an agarose gel was blue when emission was photographed without an emission filter (not shown). Thus, not surprising was that optimal detection of bleomycin was not obtained with a blue filter, even though the blue range was where peak emission was previously found for bleomycin [38]. Among the blue, green, yellow and orange filters, optimal detection was obtained with the green filter.

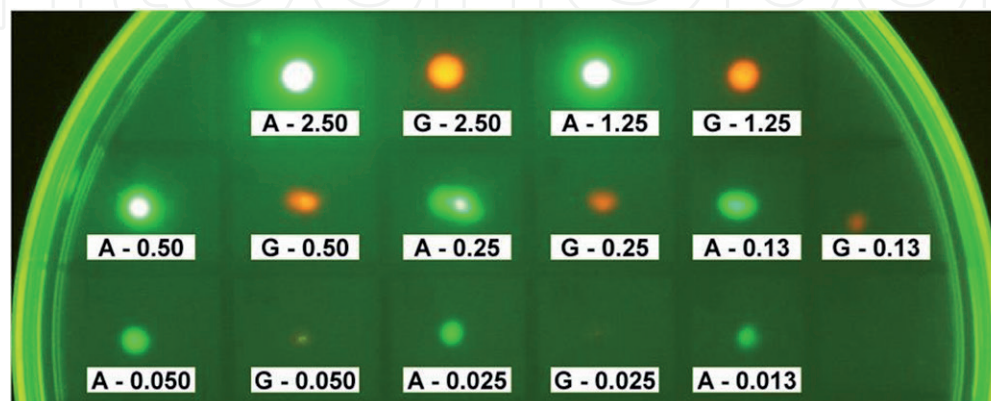


Figure 2.

Fluorescence of free GelStar. GelStar and Alexa Fluor 488 were diluted and, then, pipetted onto the surface of an agarose gel. The fluorescence was photographed through the orange filter. The GelStar samples are indicated by G, followed by the effective volume (μl) of the original, undiluted GelStar solution. The Alexa Fluor 488 samples are indicated by A, followed by the amount (μg) of Alexa Fluor 488.

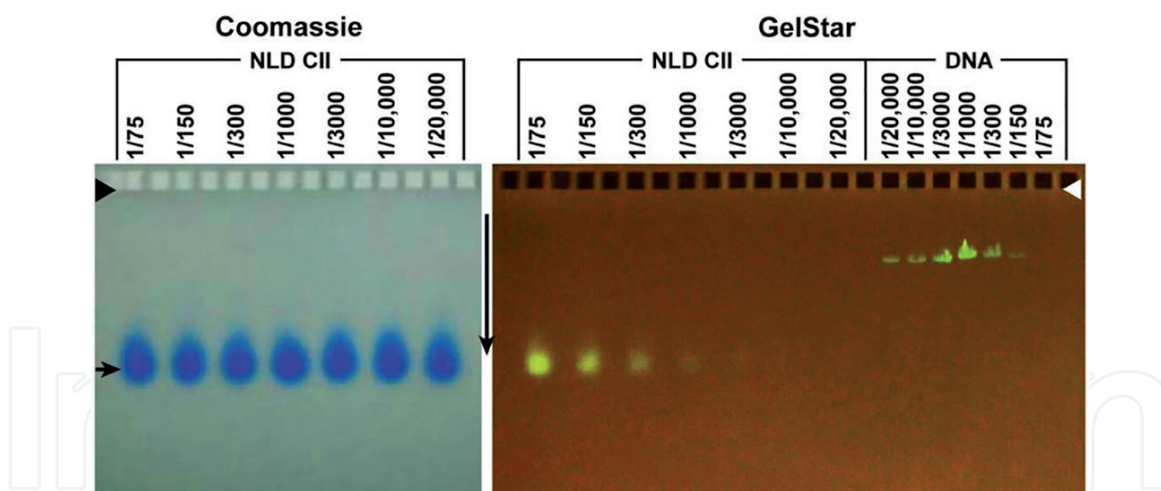


Figure 3. Association of GelStar with T₃ NLD capsid II. A commercial GelStar solution was diluted to the extent indicated above a lane and incubated with T₃ NLD capsid II. Association of GelStar with the capsid was determined by AGE, followed by, first, photography of fluorescence (right panel, lanes labeled NLD CII) and, then, staining of protein with Coomassie blue (left panel). Also analyzed was purified T₃ DNA (right panel, lanes labeled DNA), which does not stain with Coomassie blue. The arrow indicates the direction of electrophoresis; the arrowheads indicate the origins.

With the green emission filter, the minimal detected bleomycin amount was 0.2–0.4 ng when a bleomycin dilution series like the GelStar dilution series in **Figure 2** was photographed (not shown). Contrast enhancement of images was used at these lower amounts.

2.3 Loading of GelStar in NLD capsid II

We succeeded in loading GelStar into NLD capsid II. To achieve loading, 10 μ g of NLD capsid II was incubated with GelStar at 45°C. Loading was then assayed by AGE at 10°C. Then, the gel was illuminated with ultraviolet light. The result was a fluorescent band of intensity that monotonically increased with decreasing GelStar dilution (left section of the right panel of **Figure 3**). The capsid amount was invariant, as judged by Coomassie staining of the same gel (left panel of **Figure 3**). At GelStar dilutions lower than those in **Figure 3**, down to 1/10, the band intensity reached a plateau (not shown). The dominant fluorescence, at all dilutions, was green, implying that the GelStar was bound to something capsid associated. GelStar did not detectably associate with NHD capsid II (not shown).

The following data indicated that the GelStar-binding capsid site was not on a DNA molecule associated with the capsid. As the dilution of GelStar decreased, the DNA-bound GelStar fluorescence underwent, first, an increase and then a decrease (**Figure 3**, right segment of right panel). However, the decrease was not observed for the binding to NLD capsid II. Second, although a minor NLD capsid II fraction has DNA [31], the DNA-containing NLD capsid II had been excluded during purification by selecting the low-density side of the NLD capsid II band after buoyant density centrifugation in a Nycodenz density gradient. Thus, the GelStar was apparently either self-bound or bound to capsid protein.

2.4 Loading of bleomycin in NLD capsid II

Association of bleomycin with T₃ NLD capsid II was also achieved. However, the fluorescence signal was relatively weak (**Figure 4**). The bleomycin fluorescence signal of a NLD capsid II band did not change when the concentration of bleomycin was changed from 2 to 16 mg/ml. A bleomycin-associated NLD capsid II band is

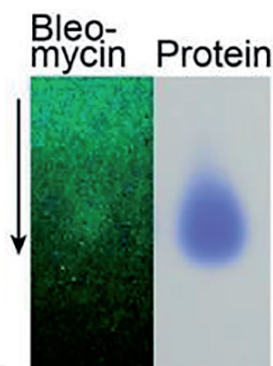


Figure 4.

Association of bleomycin with T₃ NLD capsid II. The experiment of Figure 3 was repeated with bleomycin (8 mg/ml), instead of GelStar. The capsid region of the post-AGE gel is shown. The right (protein) panel has a single band of capsid stained with Coomassie blue. This band marks the position of the capsid-associated bleomycin fluorescence in the left panel. The arrow indicates direction of electrophoresis.

shown in **Figure 4**. Most of the free bleomycin migrated toward the cathode (not shown), i.e., in a direction opposite to the direction of capsid migration.

The strength of the signal in **Figure 4** was weakened by the blue background and use of a green filter. In addition, a contaminant in the bleomycin preparation migrated close to the capsids, and is seen above the capsid band at the top of the left panel of **Figure 4**.

Calibration data for bleomycin, like the data for GelStar in **Figure 2**, were obtained. These data revealed that the amount of bleomycin loaded was 150–300 molecules per capsid.

3. Discussion

In the Introduction, we outlined a strategy that is expected to work, if we can achieve the following objectives: (1) high (~4 h) persistence of NLD capsid II in blood so that the EPR effect has time to work, (2) adequate loading and sealing of NLD capsid II and (3) tumor-specific, controlled release (de-sealing or unloading). Objective #1 is likely already achieved, given the high persistence of T3 phage. That is to say, if one considers this strategy to be engineering based, some of the engineering might already be done by natural selection.

Concerning adequate loading, the volume of the internal cavity of NLD capsid II = 6.95×10^{-17} ml. For volume occupancy (F_V) of 0.5 (equal to the F_V of DNA packaged in mature phage [34]), the number of bleomycin molecules (1416 Da; density estimated at 1.6 g/ml as sulfate) per NLD capsid II particle is 2.4×10^4 . The recommended dose of DDV-free bleomycin depends on the tumor, but is typically [39, 40] 10–20 units/m², corresponding roughly to 10–20 mg/m²; 15 mg/m² is 1.76×10^{18} bleomycin molecules/m².

To calculate the number (N_D) of NLD capsid II particles needed for this dose at $F_V = 0.5$, we initially assume a 25 g mouse, which on average, has 78.6 cm² surface area [41]. Then, N_D is 3.6×10^{11} . A 6-liter culture yields 150–300 mouse doses of this size (cost ~ \$1500), assuming (1) laboratory-scale production technique, (2) no development of procedures to increase the amount produced per bacterial cell, and (3) no drug-dose reduction caused by improved targeting. That is to say, if we can half-fill the volume of NLD capsid II, we have a viable beginning. However, thus far, we have filled no more than 2% of $F_V = 0.5$, NLD capsid II volume. So, increasing the loading is a major objective for the future.

An apparent obstacle to achieving this goal is the nonincrease in loading as bleomycin concentration increases above 2 mg/ml. At least two possible explanations

exist. (1) After passing through an open gate, the bleomycin eventually causes the gate to close. We were hoping to close the gate by lowering temperature. (2) After diffusing through an open gate, the bleomycin is prevented from diffusing in reverse by binding to internal proteins; the internal proteins become saturated as the concentration of bleomycin increases. In either case, increasing the loading is a problem of engineering.

An advantage of using a phage DDV is that the human-design engineering potential is relatively high. First of all, the capsids in a T7 NLD capsid II preparation are structurally uniform enough so that symmetric cryo-EM reconstruction is obtained at 3.5 Å [34] and asymmetric reconstruction, at ~8 Å [36]. Assuming T3 capsids to be comparably homogeneous, use of chemistry to improve gating should produce relatively uniform results.

Second, phages, in general, and phage T3 in particular, can be genetically manipulated, which is not possible with liposomes. Information for determining which nucleotides to change can be obtained from high-resolution cryo-EM structure. Structure of this type is not obtainable with liposomes.

Finally, we note that, as far as we know, the only phages tested for production of an NLD capsid II-like capsid are the related coliphages, T7, T3 and ϕ II. All three of these phages produce a NLD capsid II-like capsid [42]. Other phages are potential sources of gated capsids, perhaps with properties even more DDV-favorable.

4. Materials and methods

4.1 T3 bacteriophage, capsids and DNA (nanoparticles)

We obtained bacteriophage T3 and T3 capsid II from 30°C-lysates of host, *Escherichia coli* BB/1, that had been infected by phage T3 in aerated liquid culture [43]. The growth medium was 2× LB medium: 2.0% Bacto tryptone, 1.0% Bacto yeast in 0.1 M NaCl. We initially purified both phage and capsids by centrifugation through a cesium chloride step gradient, followed by buoyant density centrifugation in a cesium chloride density gradient [43]. The latter fractionation separates capsid I from capsid II.

To separate NLD capsid II from NHD capsid II, we performed buoyant density centrifugation of capsid II in a Nycodenz density gradient, as previously described [32]. The purified NLD and NHD capsid II were dialyzed against 0.1 M NaCl, 0.01 M Tris-Cl, pH 7.4, 0.001 M MgCl₂. NLD capsid II, which formed a band near the top of the Nycodenz density gradient, had no detected contamination with NHD capsid II and vice versa, as previously seen by analytical ultracentrifugation [31]. Phage, NLD capsid II and NHD capsid II were dialyzed against the following buffer before use in the experiments described below: 0.2 M NaCl, 0.01 M Tris-Cl, pH 7.4, 0.001 MgCl₂.

T3 DNA was obtained from purified T3 phage by phenol extraction. The DNA was dialyzed against and stored in 0.1 M NaCl, 0.01 M Tris-Cl, pH 7.4, 0.001 M EDTA. DNA concentration was obtained from optical density at 260 nm.

4.2 Fluorescent compounds: test of fluorescence emission

GelStar was obtained from Lonza (Basel, Switzerland) in solution. The company recommends dilution by a factor of 1:10,000 for use as a nucleic acid stain after gel electrophoresis. Alexa Fluor 488 succinimidyl ester was obtained from Molecular Probes (Eugene, OR, USA) as a powder.

Bleomycin was obtained from Cayman Chemical Company (Ann Arbor, MI, USA) as a powder. The bleomycin was dissolved in the aqueous buffer indicated and diluted to the concentrations indicated before incubation with capsids and DNA.

Tests of fluorescence emission vs. fluorescent molecule concentration were made by pipetting 5 μ l of diluted fluorescent molecule onto the surface of a 0.7% agarose gel (LE agarose, Lonza) that had been cast in a plastic Petri dish in the electrophoresis buffer of Section 4.3. The gel was then photographed by use of the procedures described in Section 4.3.

4.3 Loading experiments: AGE

To test for fluorescent compound/nanoparticle association, fluorescent compounds were mixed with one of the following T3 nanoparticles: NLD capsid II, NHD capsid II, phage, DNA. First, a 12.5 μ l amount of fluorescent compound in 0.1 M NaCl, 0.01 M sodium citrate, pH 4.0, 0.001 M MgCl₂ (citrate buffer) was added to 4.5 μ l of additional citrate buffer. Then, 8.0 μ l of a nanoparticle sample was added and mixed (final pH, 4.1). This mixture was incubated at 45.0°C for 2.0 h.

To perform AGE, we added to this mixture 2.5 μ l of the following solution: 60% sucrose (to increase the density for layering in sample wells) in the electrophoresis buffer below. This final mixture was layered in a well of a horizontal, submerged, 0.7% agarose gel (LE agarose, Lonza), cast in and submerged under the following electrophoresis buffer: 0.05 M Tris-acetate, pH 8.4, 0.001 M MgCl₂. The temperature of the gel and buffer had been pre-adjusted to 10°C in an effort to seal NLD capsid II and, therefore, prevent leakage of fluorescent compounds.

AGE was performed at 1.0 V/cm for 18.0 h with the gel and buffer maintained at 10°C by circulation through a controlled-temperature water bath. After AGE, the gel was soaked in 25% methanol in electrophoresis buffer for 1.5 h at room temperature, to cause leakage of fluorescent compounds from NLD capsid II and, therefore, to prevent auto-quenching.

Finally, the gel was photographed during illumination with a Model TM-36 ultraviolet transilluminator (Ultra Violet Products, Inc.). The camera used was a Canon Power Shot G2, 4.0 Megapixels. The following Tiffin emission filters were used as described in Section 2: Blue, 80A #290513; Green, 11Green 1—#287305; Yellow, Yellow 12—#282224; Orange, Orange 16—#289750. To detect capsid protein, the gel was subsequently stained with Coomassie blue and photographed during illumination with visible light [43].

5. Conclusions

Obtaining an increase in the current tumor-specificity of anticancer drugs should be possible via use of a DDV that implements multiple, independent stages of specificity increase. T3 NLD capsid II is an example of a bio-nanoparticle that has undergone some of the needed DDV-bioengineering via mutation/selection in the environment. Other examples, not yet found, are assumed to exist and potentially have even more favorable characteristics.

Acknowledgements

The authors acknowledge support from the San Antonio Area Foundation and the Morrison Trust.

Conflict of interest

The authors declare no conflict of interest.

IntechOpen

IntechOpen

Author details

Philip Serwer*, Elena T. Wright and Cara B. Gonzales
The University of Texas Health Science Center, San Antonio, Texas, USA

*Address all correspondence to: serwer@uthscsa.edu

IntechOpen

© 2020 The Author(s). Licensee IntechOpen. This chapter is distributed under the terms of the Creative Commons Attribution License (<http://creativecommons.org/licenses/by/3.0>), which permits unrestricted use, distribution, and reproduction in any medium, provided the original work is properly cited. 

References

- [1] Park GT, Choi KC. Advanced new strategies for metastatic cancer treatment by therapeutic stem cells and oncolytic virotherapy. *Oncotarget*. 2016;**7**:58684-58695. DOI: 10.18632/oncotarget.11017
- [2] Leaf C. *The Truth in Small Doses: Why We're Losing the War on Cancer—And How to Win It*. New York: Simon and Schuster; 2014
- [3] Hanahan D. Rethinking the war on cancer. *The Lancet*. 2014;**383**:558-563. DOI: 10.1016/S0140-6736(13)62226-6
- [4] Mamdouhi T, Twomey JD, Mc Sweeney KM, Zhang B. Fugitives on the run: Circulating tumor cells (CTCs) in metastatic disease. *Cancer Metastasis Reviews*. 2019;**38**:297-305. PMID: 27683421
- [5] Lambert AW, Pattabiraman DR, Weinberg RA. Emerging biological principles of metastasis. *Cell*. 2017;**168**:670-691. DOI: 10.1016/j.cell.2016.11.037
- [6] Chabner BA, Roberts TG Jr. Timeline: Chemotherapy and the war on cancer. *Nature Reviews Cancer*. 2005;**5**:65-72. DOI: 10.1038/nrc1529
- [7] Nurgali K, Jagoe RT, Abalo R. Editorial: Adverse effects of cancer chemotherapy: Anything new to improve tolerance and reduce sequelae? *Frontiers in Pharmacology*. 2018;**9**: 245. DOI: 10.3389/fphar.2018.00245
- [8] DeVita VT Jr, Chu E. A history of cancer chemotherapy. *Cancer Research*. 2008;**68**:8643-8653. DOI: 10.1158/0008-5472.CAN-07-6611
- [9] Inthagard J, Edwards J, Roseweir AK. Immunotherapy: Enhancing the efficacy of this promising therapeutic in multiple cancers. *Clinical Science (London, England)*. 2019;**133**:181-193. DOI: 10.1042/CS20181003
- [10] Christofi T, Baritaki S, Falzone L, Libra M, Zaravinos A. Current perspectives in cancer immunotherapy. *Cancers (Basel)*. 2019;**11**:E1472. DOI: 10.3390/cancers11101472
- [11] Marshall HT, Diamgoz MBA. Immuno-oncology: Emerging targets and combination therapies. *Frontiers in Oncology*. 2018;**8**:315. DOI: 10.3389/fonc.2018.00315
- [12] Schae D, McBride WH. Opportunities and challenges of radiotherapy for treating cancer. *Nature Reviews Clinical Oncology*. 2015;**12**:527-540. DOI: 10.1038/nrclinonc.2015.120
- [13] Chen HHW, Kuo MT. Improving radiotherapy in cancer treatment: Promises and challenges. *Oncotarget*. 2017;**8**:62742-62758. DOI: 10.18632/oncotarget.18409
- [14] Baskar R, Lee KA, Yeo R, Yeoh KW. Cancer and radiation therapy: Current advances and future directions. *International Journal of Medical Sciences*. 2012;**9**:193-199. DOI: 10.7150/ijms.3635
- [15] Zhang Y, Liu Z. Oncolytic virotherapy for malignant tumor: Current clinical status. *Current Pharmaceutical Design*. 2019. DOI: 10.2174/1381612825666191104090544 [Epub ahead of print]
- [16] Lawler SE, Speranza MC, Cho CF, Chiocca EA. Oncolytic viruses in cancer treatment: A review. *JAMA Oncology*. 2017;**3**:841-849. DOI: 10.1001/jamaoncol.2016.2064
- [17] Serwer P, Wright ET. Nanomedicine and phage capsids. *Viruses*. 2018;**10**: E307. DOI: 10.3390/v10060307
- [18] Bloch H. Experimentelle untersuchungen über beziehungen zwischen bakterioophagen und malignen

tumoren. *Archiv fur die Gesamte Virusforschung*. 1940;**1**:481-496. DOI: 10.1007/BF01240654

[19] Budynek P, Dąbrowska K, Skaradziński G, Górski A. Bacteriophages and cancer. *Archives of Microbiology*. 2010;**192**:315-320. DOI: 10.1007/s00203-010-0559-7

[20] Kalyane D, Raval N, Maheshwari R, Tambe V, Kalia K, Tekade RK. Employment of enhanced permeability and retention effect (EPR): Nanoparticle-based precision tools for targeting of therapeutic and diagnostic agent in cancer. *Materials Science & Engineering. C, Materials for Biological Applications*. 2019;**98**:1252-1276. DOI: 10.1016/j.msec.2019.01.066

[21] Fang J, Islam R, Islam W, Yin H, Subr V, Etrych T, et al. Augmentation of EPR Effect and Efficacy of anticancer nanomedicine by carbon monoxide generating agents. *Pharmaceutics*. 2019;**11**:343. DOI: 10.3390/pharmaceutics11070343

[22] Anchordoquoy TJ, Barenholz Y, Boraschi D, Chorny M, Decuzzi P, Dobrovolskaia MA, et al. Mechanisms and barriers in cancer nanomedicine: Addressing challenges, looking for solutions. *ACS Nano*. 2017;**11**:12-18. DOI: 10.1021/acsnano.6b08244

[23] Barenholz Y. Doxil[®]—The first FDA-approved nano-drug: Lessons learned. *Journal of Controlled Release*. 2012;**160**:117-134. DOI: 10.1016/j.jconrel.2012.03.020

[24] Silverman L, Barenholz B. In vitro experiments showing enhanced release of doxorubicin from Doxil[®] in the presence of ammonia may explain drug release at tumor site. *Nanomedicine*. 2015;**11**:1841-1850. DOI: 10.1016/j.nano.2015.06.007

[25] Nakamura Y, Mochida A, Choyke PL, Kobayashi H. Nanodrug

delivery: Is the enhanced permeability and retention effect sufficient for curing cancer? *Bioconjugate Chemistry*. 2016;**27**:2225-2238. DOI: 10.1021/acs.bioconjchem.6b00437

[26] Gopalakrishna P. Nanomedicines for cancer therapy: An update of FDA approved and those under various stages of development. *SOJ Pharmacy and Pharmaceutical Sciences*. 2014;**1**:13. DOI: 10.15226/2374-6866/1/2/00109

[27] Abraham SA, Waterhouse DN, Mayer LD, Cullis PR, Madden TD, Bally MB. The liposomal formulation of doxorubicin. *Methods in Enzymology*. 2005;**39**:71-96. DOI: 10.1016/S0076-6879(05)91004-5

[28] Kanwal U, Irfan Bukari N, Ovais M, Abass N, Hussain K, Raza A. Advances in nano-delivery systems for doxorubicin: An updated insight. *Journal of Drug Targeting*. 2018;**26**:296-310. DOI: 10.1080/1061186X.2017.1380655

[29] Gabizon A, Martin F. Polyethylene glycol-coated (pegylated) liposomal doxorubicin. Rationale for use in solid tumours. *Drugs*. 1997;**54**(Suppl. 4):15-21. DOI: 10.2165/00003495-199700544-00005

[30] Serwer P, Wright E, Lee JC. High murine blood persistence of phage T3 and suggested strategy for phage therapy. *BMC Research Notes*. 2019;**12**:560. DOI: 10.1186/s13104-019-4597-1

[31] Serwer P, Wright ET, Demeler B, Jiang W. States of T3/T7 capsids: Buoyant density centrifugation and cryo-EM. *Biophysical Reviews*. 2018;**10**:583-596. DOI: 10.1007/s12551-017-0372-5

[32] Serwer P, Wright ET, Chang J, Liu X. Enhancing and initiating phage-based therapies. *Bacteriophage*. 2014;**4**:e961869. DOI: 10.4161/21597073.2014.961869

- [33] Khan SA, Griess GA, Serwer P. Assembly-associated structural changes of bacteriophage T7 capsids. Detection by use of a protein-specific probe. *Biophysical Journal*. 1992;**63**:1286-1292. DOI: 10.1016/S0006-3495(92)81724-1
- [34] Guo F, Liu Z, Fang P-A, Zhang Q, Wright E, Wu W, et al. Capsid expansion mechanism of bacteriophage T7 revealed by multistate atomic models derived from cryo-EM reconstructions. *Proceedings of the National Academy of Sciences of the United States of America*. 2014;**111**:E4606-E4614. DOI: 10.1073/pnas.1407020111
- [35] Serwer P. A metrizamide-impermeable capsid in the DNA packaging pathway of bacteriophage T7. *Journal of Molecular Biology*. 1980;**138**:65-91. DOI: 10.1016/S0022-2836(80)80005-2
- [36] Guo F, Liu Z, Vago F, Ren Y, Wu W, Wright ET, et al. Visualization of uncorrelated tandem symmetry mismatches in the internal genome packaging apparatus of phage T7. *Proceedings of the National Academy of Sciences of the United States of America*. 2013;**110**:6811-6816. DOI: 10.1073/pnas.1215563110
- [37] Watson RA, De La Pena H, Tsakok MT, Joseph J, Stoneham S, Shamash J, et al. Development of a best-practice clinical guideline for the use of bleomycin in the treatment of germ cell tumours in the UK. *British Journal of Cancer*. 2018;**119**:1044-1051. DOI: 10.1038/s41416-018-0300-x
- [38] Motlagh NS, Parvin P, Ghasemi F, Atyabi F. Fluorescence properties of several chemotherapy drugs: Doxorubicin, paclitaxel and bleomycin. *Biomedical Optics Express*. 2016;**7**:2400-2406. DOI: 10.1364/BOE.7.002400
- [39] Medscape, bleomycin (Rx). 2019. Available from: <https://reference.medscape.com/drug/bleomycin-342113>
- [40] Drugs.com. 2019. Available from: <https://www.drugs.com/dosage/bleomycin.html>
- [41] Dawson NJ. The surface-area/body-weight relationship in mice. *Australian Journal of Biological Sciences*. 1967;**20**:687-690. ISSN: 0004-9417
- [42] Serwer P, Watson RH, Hayes SJ, Allen JL. Comparison of the physical properties and assembly pathways of the related bacteriophages T7, T3 and phi II. *Journal of Molecular Biology*. 1983;**170**:447-469. DOI: 10.1016/S0022-2836(83)80157-0
- [43] Serwer P, Wright ET, Liu Z, Jiang W. Length quantization of DNA partially expelled from heads of a bacteriophage T3 mutant. *Virology*. 2014;**456-457**:157-170. DOI: 10.1016/j.virol.2014.03.016